Comparison of the 14.1 MeV Neutron Instrument Response Function and Counting Efficiencies for NTF22D with Quartz and EJ228, EJ232Q (1%) scintillators

SAND2018-13656PE

Jedediah Styron, Research Faculty
Dept. of Nuclear Engineering
University of New Mexico

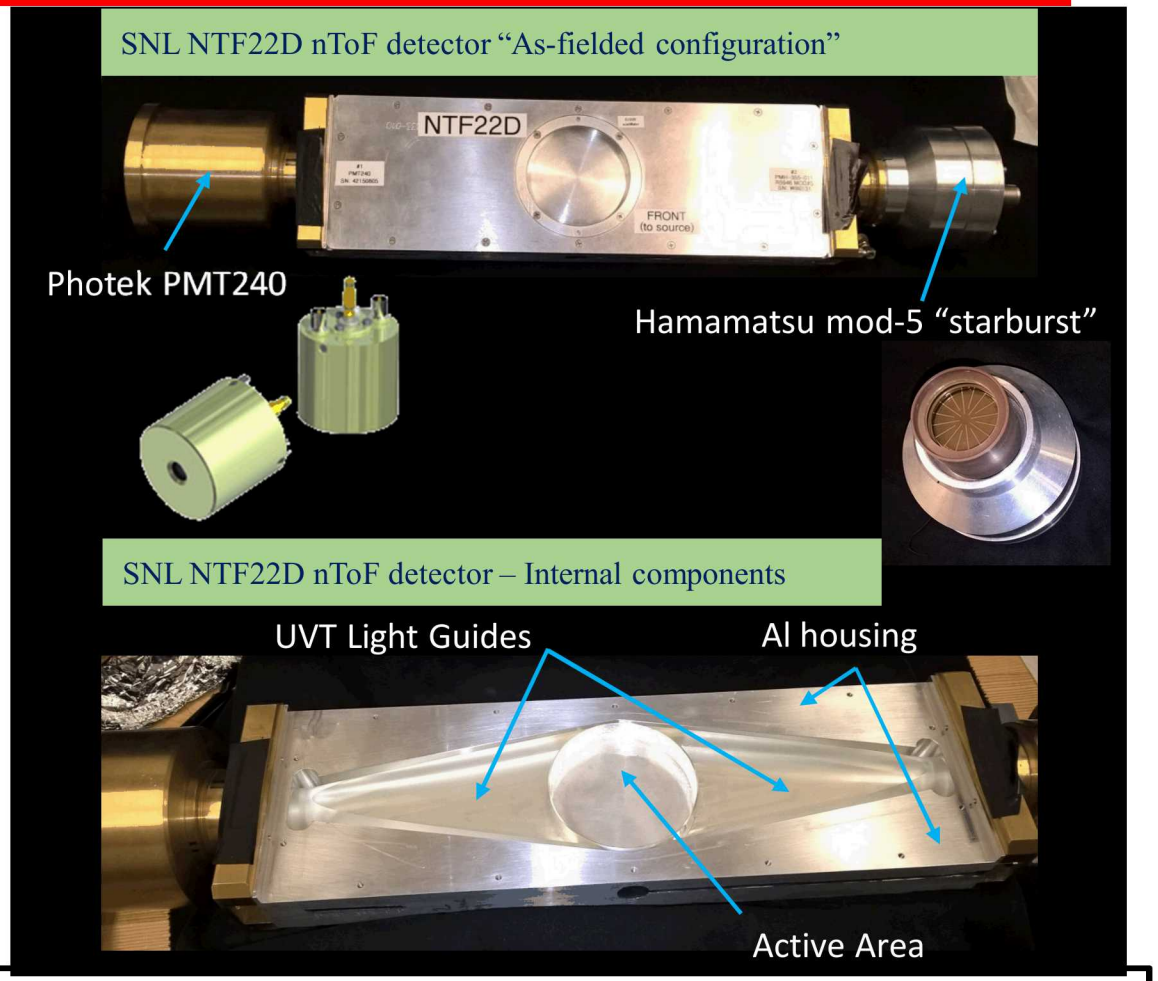

nToF Diagnostic Working Group Meeting
University of Rochester – Laboratory for Laser Energetics
December 4, 2018

Sandia National Laboratories is a multimission laboratory managed and operated by National Technology and Engineering Solutions of Sandia, LLC., a wholly owned subsidiary of Honeywell International, Inc., for the U.S. Department of Energy's National Nuclear Security Administration under contract DE-NA-0003525.

Collaborators

- University of New Mexico
  - Gary Cooper
  - Sara Pelka
  - Jeremy Vaughan
  - Colin Weaver
- Sandia National Laboratories
  - Carlos Ruiz
  - Gordon Chandler
  - Bruce McWatters
  - Jose Torres
  - Brent Jones
  - Clark Highstrete
- Lawrence Livermore National Laboratories
  - Kelly Hahn
- National Nuclear Security Site
  - Ken Moy
  - Robert Buckles

Summary

- The instrument response function (IRF) and average neutron sensitivity have been determined for the same detector using EJ228 and EJ232Q-1% scintillators and quartz over a broad dynamic range using an average of single-event DT neutron interactions.
- The response characteristics of each material (pulse shape, width, amplitude, area) agree with the expected values.
- A path forward to convert single-event IRFs to current integrated has been developed

Outline

- Experimental geometry at the IBL
- IRF analysis procedure
- Comparison of scintillation materials (EJ228,EJ232Q-1%) and Quartz
- Experimental results
- Single-event to current integrated
- Conclusions

nToF detectors can be characterized using the neutron calibration chamber (NUCAL) at the Ion Beam Laboratory (IBL).

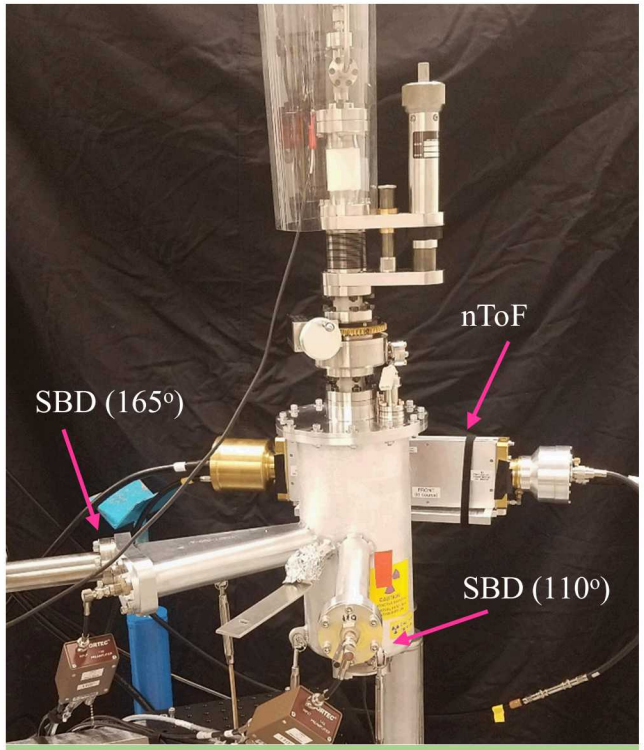

NUCAL target chamber, shown with a dual PMT nToF under study

- Ion beam generated using a 350 keV Cockroft-Walton HVEE accelerator
  - Magnetically analyzed beam
  - Electrostatic focusing
  - Electromagnetic steering

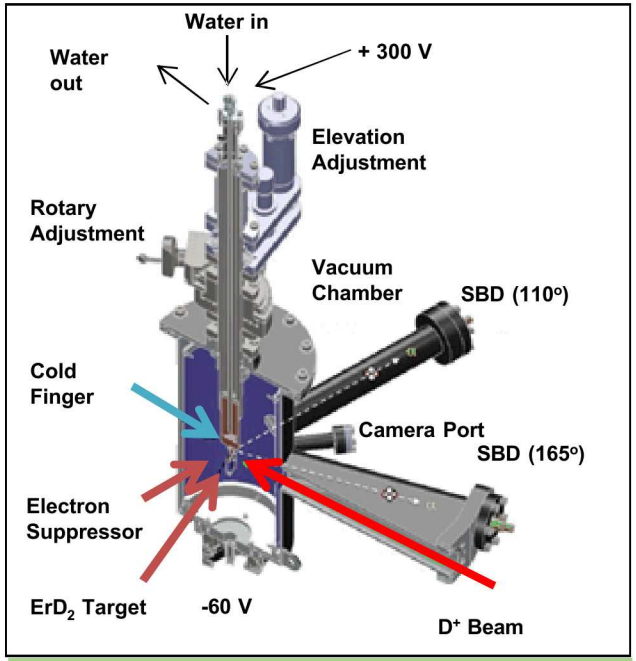

Schematic of the NUCAL target chamber

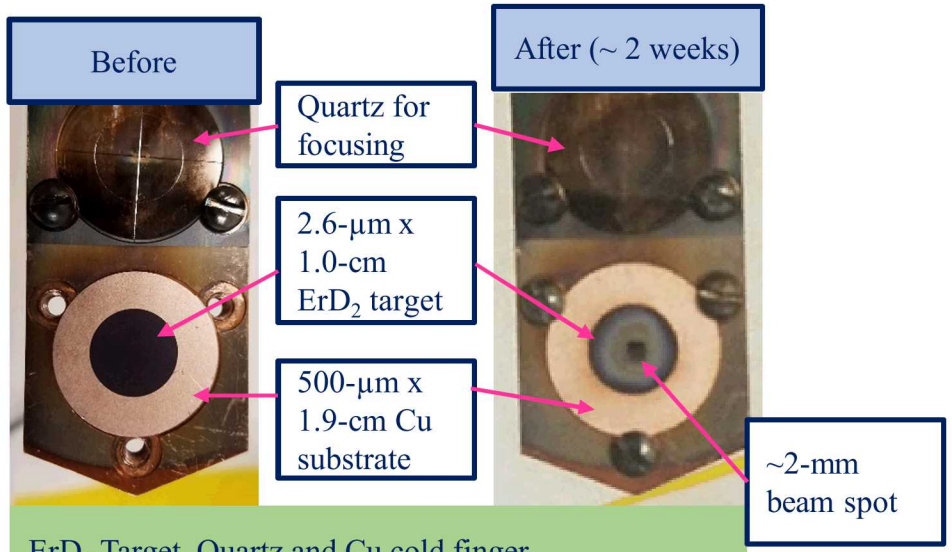

ErD$_2$ Target, Quartz and Cu cold finger

C. L. Ruiz et al., Rev. Sci. Instrum. **83**, 10D913 (2012)

Particle coincidence is derived from the reaction kinematics and used to infer the detector response to single DT neutron interactions and the counting efficiency.

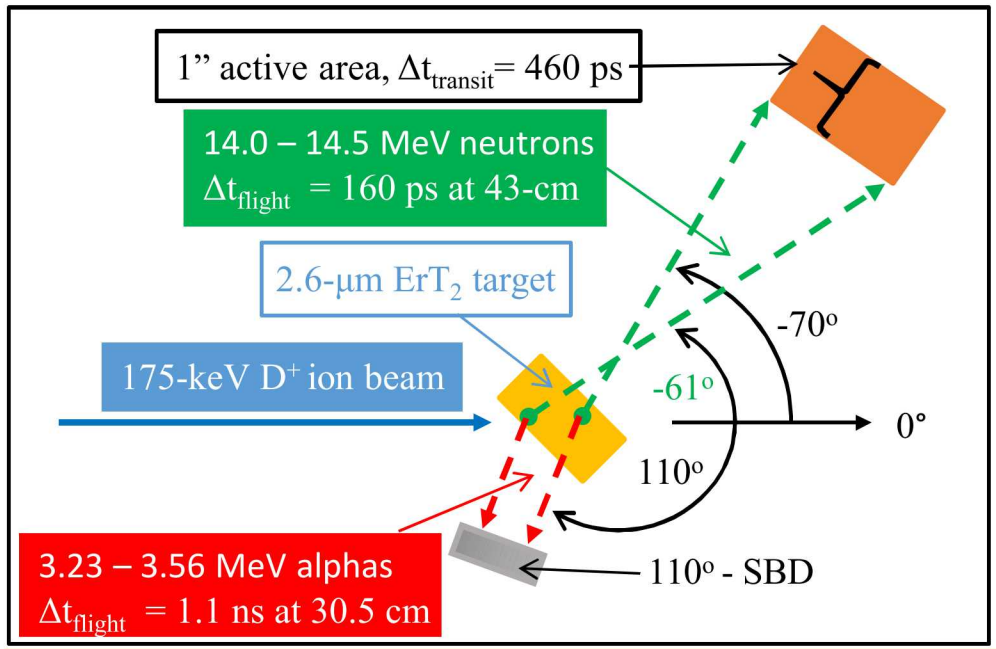

Kinematic relationship for an alpha particle emitted into an angle of 110-degrees

$$\epsilon_{ntof}\Big|_{disc} = \frac{Cts_{coin}}{Cts_{SBD}}$$

Neutron counting efficiency at a set discriminator level

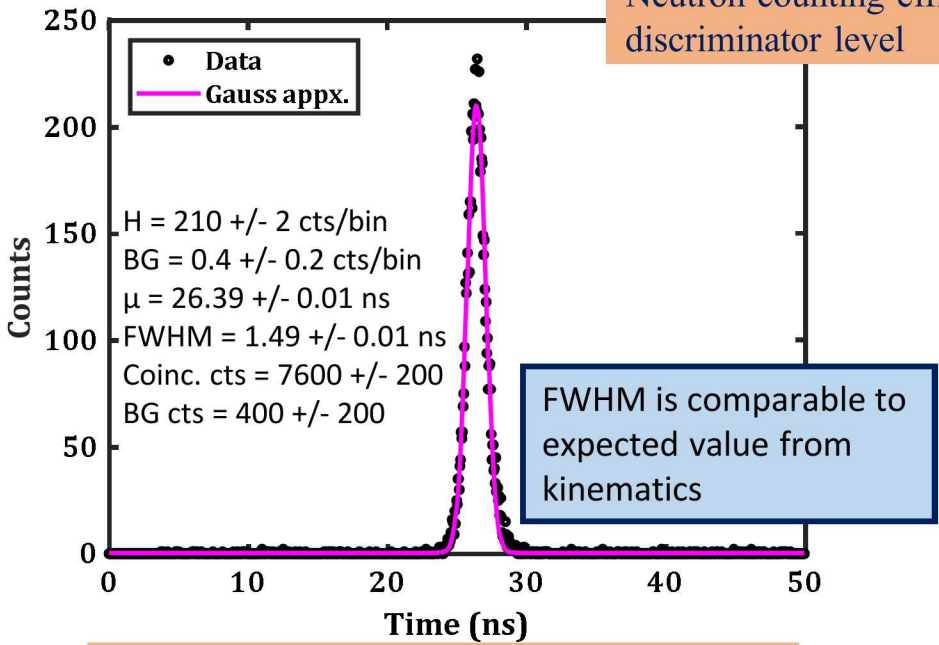

FWHM is comparable to expected value from kinematics

n-alpha coincidence curve for NTF22D w/ EJ228, Photek PMT240 at -4.0 kV

J. D. Styron et al., Rev. Sci. Instr., **89** (2018).

The IRF is an average of the leading-edge normalized data (10% of the max) , which can be described using an exponentially modified Gaussian function.

T. J. Murphy et al., Rev. Sci. Instr. **68**, 610 (1997)
J. D. Styron et al., Rev. Sci. Instr., **89** (2018).

$$IRF(t,\mu,\tau,\sigma,A) = A * \exp\left(-\frac{t-\mu}{\tau}\right) * \exp\left(\frac{\sigma^2}{2\tau^2}\right) * \left(1 + \operatorname{erf}\left(\frac{t-\mu-\frac{\sigma^2}{\tau}}{\sqrt{2\sigma^2}}\right)\right)$$

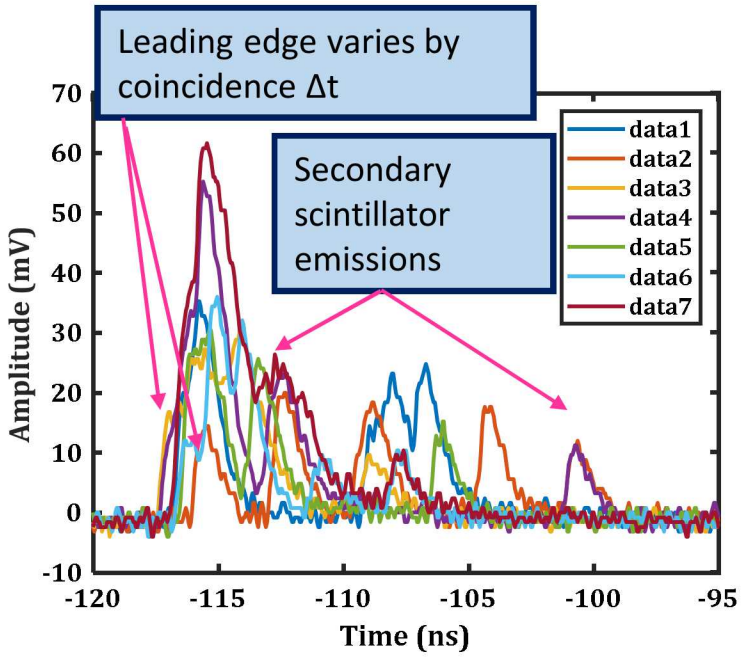

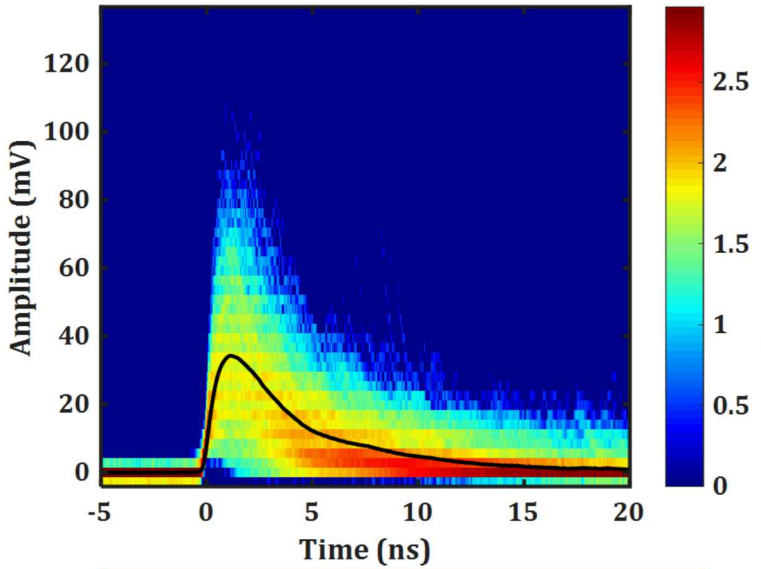

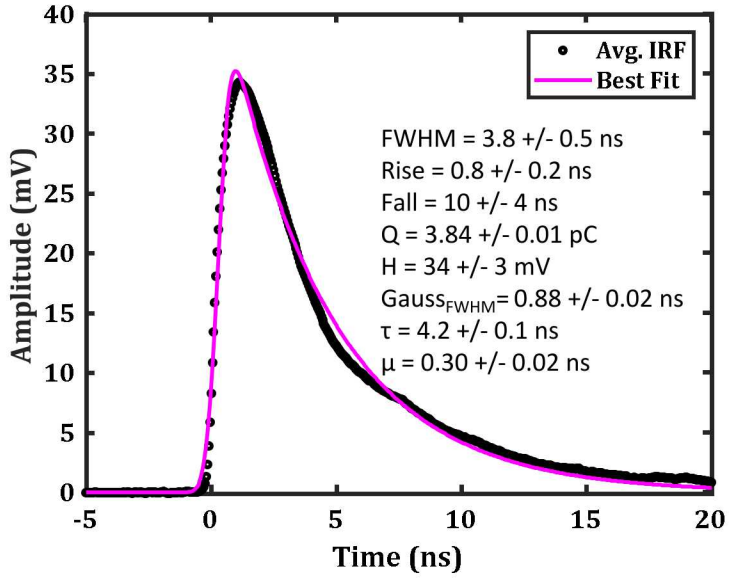

Seven waveforms shown "as-acquired"

~1000 acquisitions are normalized in time and averaged.

The average IRF is fit with a function so parameters can be compared

Detector materials are chosen based on inherent properties such as timing characteristics or neutron sensitivity.

Plastic Scintillator (1.1 H – C ratio)

- Primary reactions
  - H(n, el)H or C(n, el)C
- dE/dx conversion to electronic states (prompt and delayed)
- Isotropic visible light produced
  - 340 – 440 nm
- Light output vs. proton energy
  - $MeV_{ee} = -10.68\left(1 - e^{-0.07E^{0.89}}\right) + 0.929E$
    - $MeV_{ee}^{7MeV} = 3.01,\ MeV_{ee}^{1.25MeV} = 0.29$
- Two types of scintillators used at SNL
  - EJ228
    - $L_y^{EJ228} = \frac{10200\gamma's}{MeV_{ee}}, \Delta t = 1.2\ ns, \tau = 1.4\ ns$
  - EJ232Q-1%
    - $L_y^{EJ232} = \frac{1700\gamma's}{MeV_{ee}}, \Delta t = 290\ ps, \tau = 700\ ps$

Quartz (SiO_2)

- Primary reactions
  - n, n' or n, γ
- Cherenkov light produced by Compton scattered electrons in the quartz
- Light cone produced along e- velocity vector

$$\cos(\theta) = \frac{1}{\beta n}$$

- Electron energy threshold (n = 1.55, ρ = 2.65 g/cc)
  - $T_{th} = 0.511\left(\frac{n}{\sqrt{n^2-1}} - 1\right) = 161\ keV$
- Cherenkov photons produced per unit wavelength per path length
  - $\frac{d^2N}{dxd\lambda} = \frac{2\pi\alpha}{\lambda^2}\left(1 - \frac{1}{\beta^2 n(\lambda^2)}\right) \approx \frac{1}{\lambda^2}$
  - ~ 400 Cherenkov photons per 1-MeV electron in 300 – 600 nm range
  - $\Delta t = \delta(t), \tau = 0\ ns$

B.D Sowerby, Nucl. Instr. Meth., **97**, (1971).
J.B. Birks, The Theory and Practice of Scintillation Counting, Oxford: Pergamon Press, 1964.
Noel R. Stanton, "A Monte Carlo program for calculating neutron detection efficiencies in plastic scintillator," 1971.
Eljen Technologies, "Plastic Scintilators," 2016. [Online]. Available: http://www.eljentechnology.com/products/plastic-scintillators.

Qualitative comparison (at three different bias settings) of the three active detection materials exposed to DT neutrons exhibit the expected trends.

- The Quartz IRF is much faster than either scintillator since there is no time required to populate electronic states.
- The quenching agent in the EJ232Q-1% scintillator provides a ~1-2ns improvement over the EJ228 scintillator
  - Eljen quotes a FWHM and decay time of 1.2ns and 1.4ns for the EJ228 and 290ps and 700ps for EJ232Q-1%, respectively.

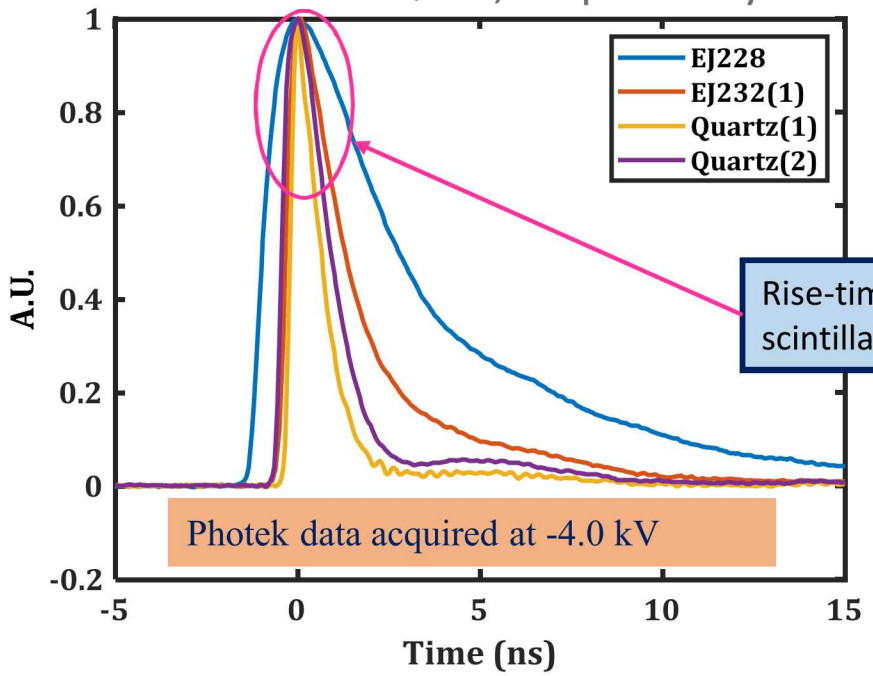

Rise-time increased due to scintillation time

Reduction in decay and width parameters

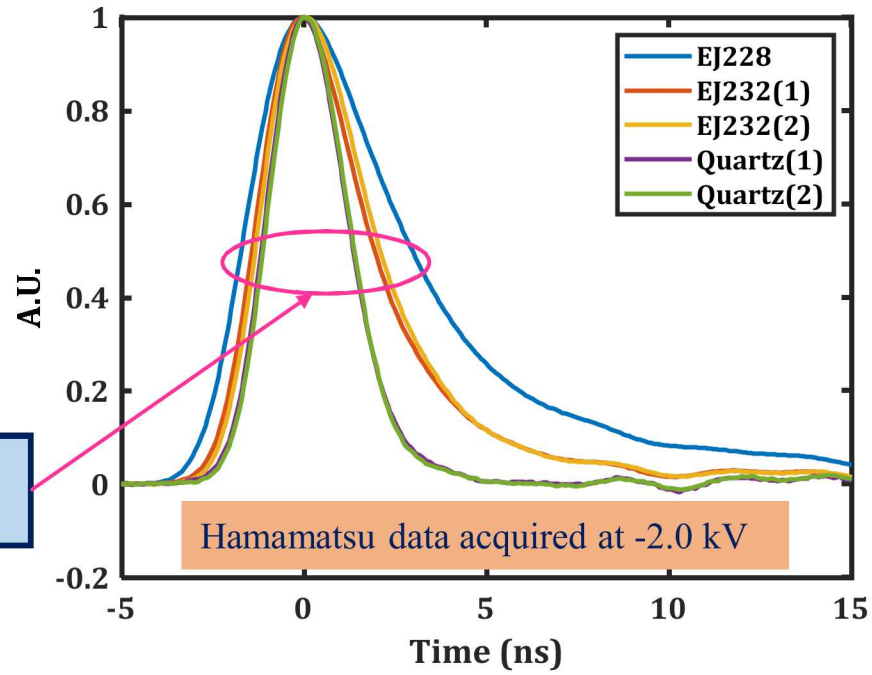

Quantitatively the IRF-FWHM parameter can be compared for each material.

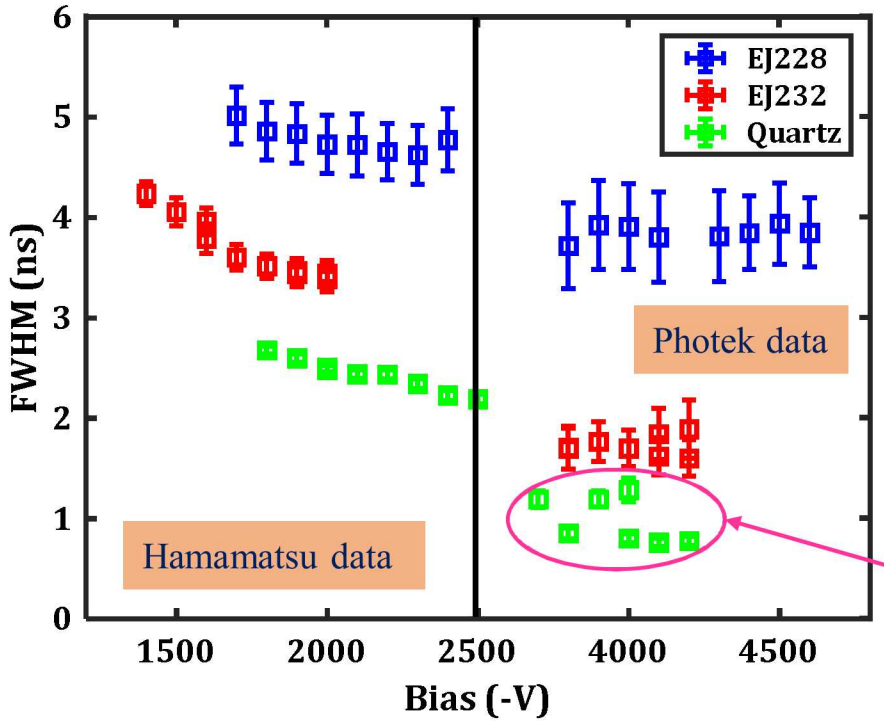

- The FWHM of the measured IRF using different material is consistent with the expected value
- The slope of each data set is consistent regardless of the detection media or source.
- The Quartz data is comparable to the PMT response

Systematic differences need to be resolved in the analysis of the data due to anomalous single-events in the data

Quantitatively the amplitude and extracted charge agree with the expected values.

- For the same particle type the EJ232Q-1% produces a factor of 6 less light than the EJ228
- The integrated charge for the Quartz with a DT source is comparable to EJ228 with a DD source (light output correlation from Verbinski et al and Stanton et al.)
  - Since we have a better understanding of scintillator this may help with scaling when fielded on Z

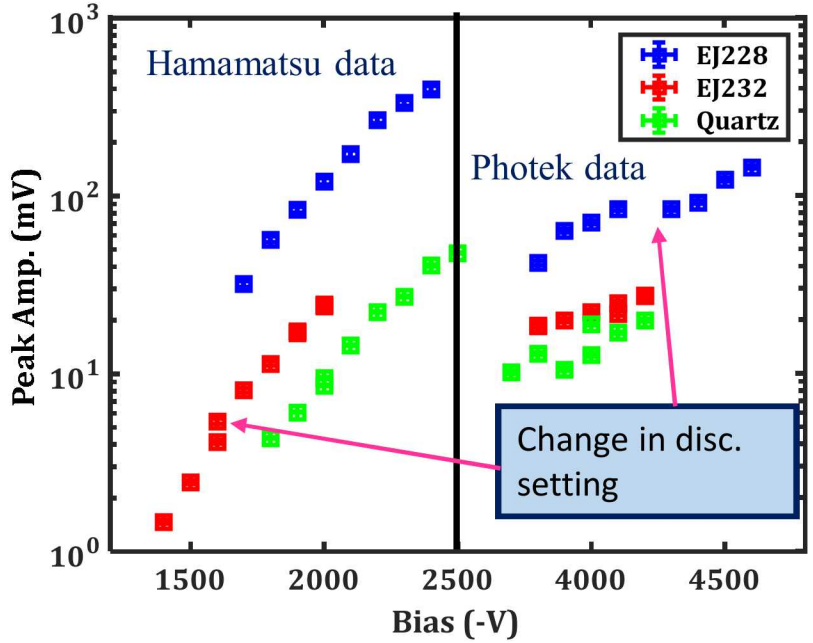

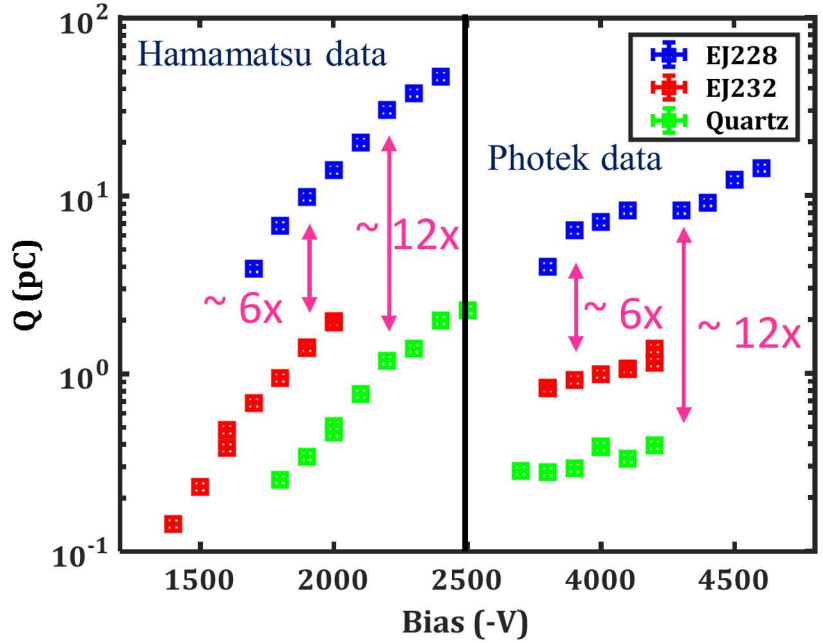

The fit parameters from the IRF function reflect the expected behavior in the measured values.

- The Gaussian FWHM from the IRF fit is consistent between data sets.
  - This implies that the Gaussian FWHM is solely due to the PMT response and not the detection media.
- The Tau parameter (scintillator decay) varies based on the detection media.
  - Given the previous statement this implies that the IRF broadening is from the scintillator

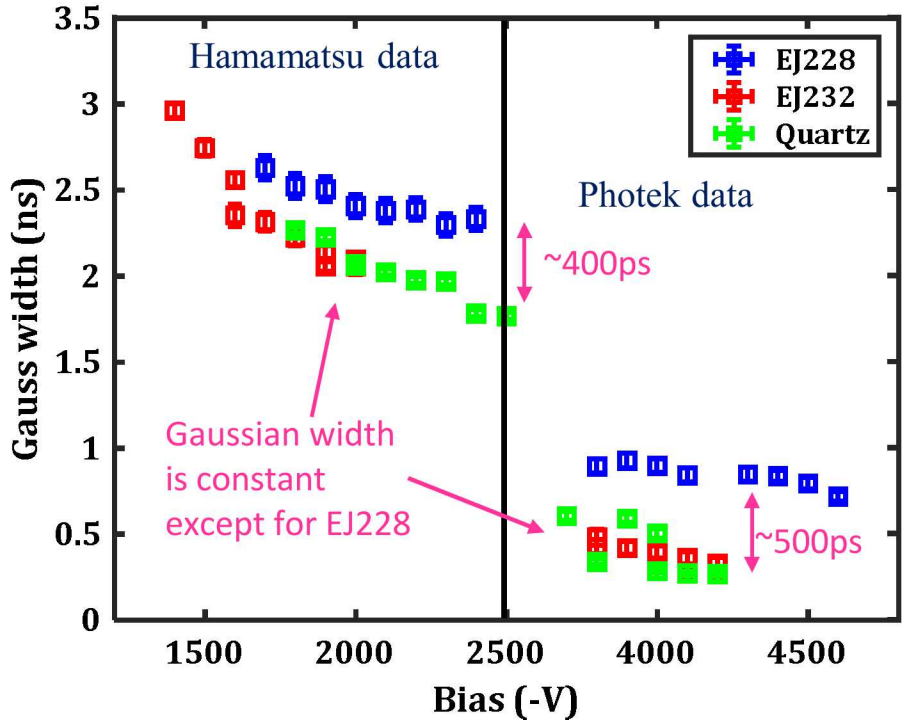

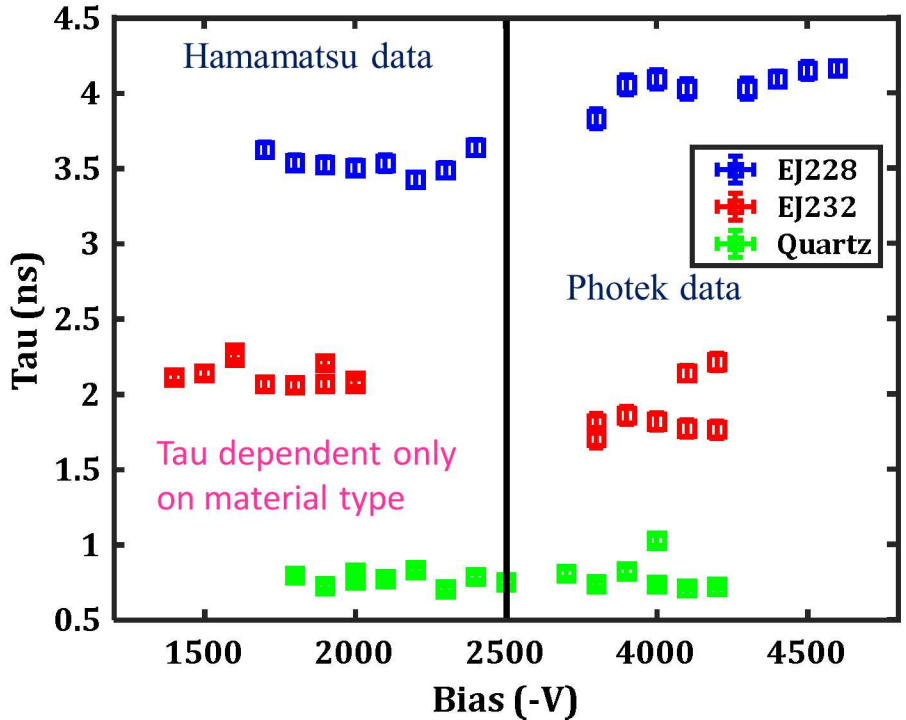

The calculated efficiencies provide a path forward to convert single-event response to current integrated.

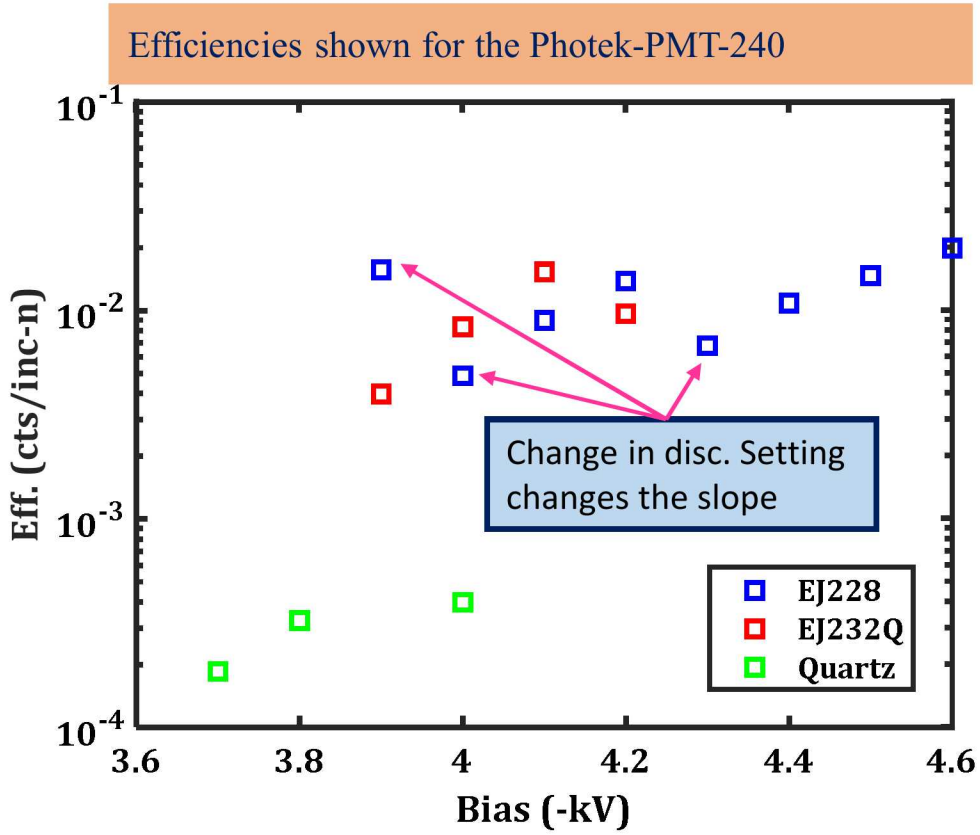

- For the scintillator materials the counting efficiency can be used to convert the sensitivity (pC/n) from single-event to current integrated
  - Differential cross-sections and light-output relationships are well known quantities for H-C scintillators
- Converting the quartz data from single-event to current integrated will require much more effort.
  - Physics are more complex with n-gamma, gamma-electron interactions.

These parameters can be converted from single-event to current integrated by using the measured and expected values for Q and the efficiency.

Conversion from single-event to integrated average sensitivity

$$Q_{int} = \frac{Q_{meas}}{Ly_{meas}} < Ly >$$

Average expected light-output

$$< Ly > = \sum_{E=0}^{E_{max}} Ly \left(\frac{dn}{dE}\right) / \sum_{E=0}^{E_{max}} \left(\frac{dn}{dE}\right)$$

Average measured light-output

$$Ly_{meas} = \sum_{E_{min}}^{E_{max}} Ly \left(\frac{dn}{dE}\right) / \sum_{E_{min}}^{E_{max}} \left(\frac{dn}{dE}\right)$$

Cumulative efficiency curve

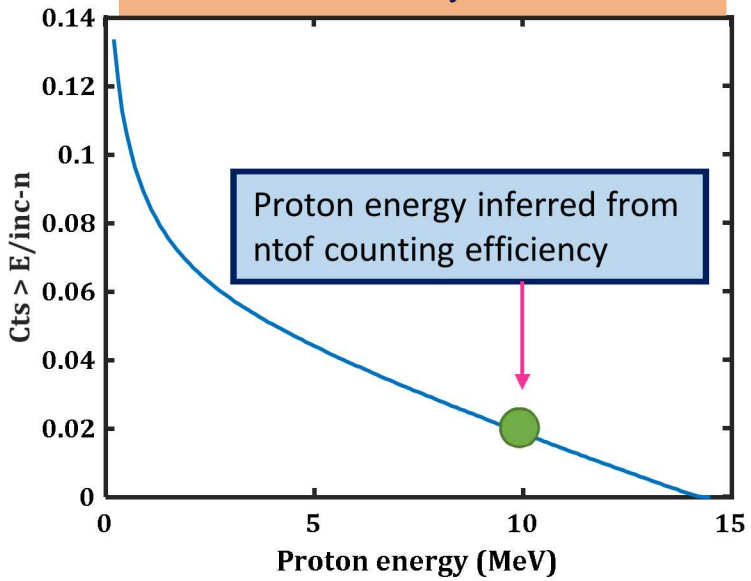

Differential efficiency curve

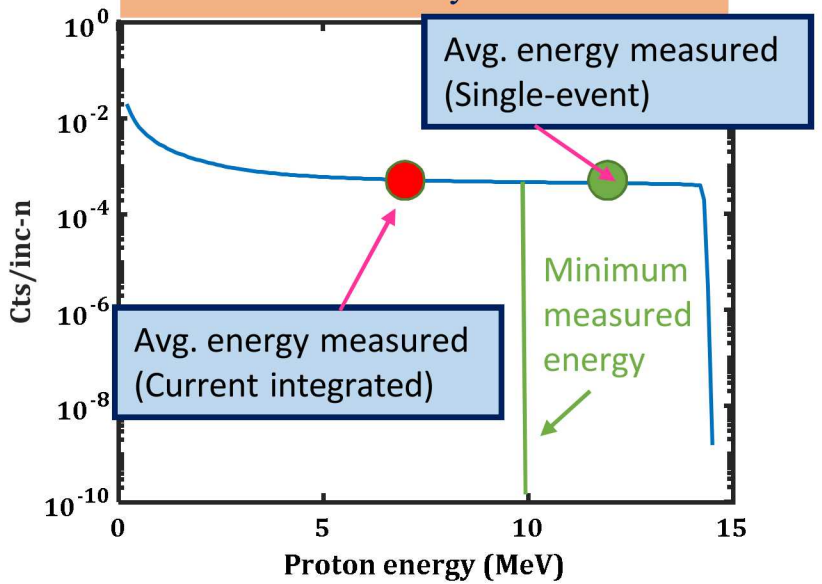

Expected proton light output

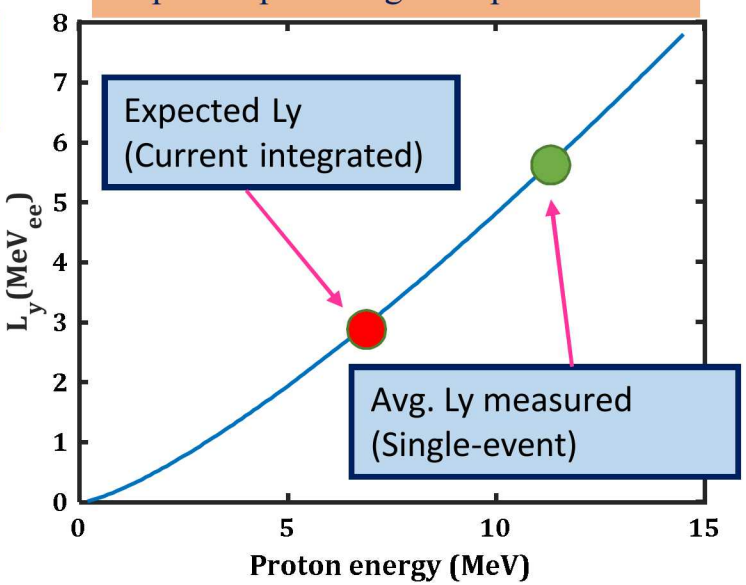

Hypothetical curves generated using n-p differential scattering cross-sections for an expected neutron flux. Assumes all protons are measured individually (Not exactly correct, for demonstration purposes only)

Summary

- The instrument response function (IRF) and average neutron sensitivity have been determined for the same detector using EJ228 and EJ232Q-1% scintillators and quartz over a broad dynamic range using an average of single-event DT neutron interactions.
- The response characteristics of each material (pulse shape, width, amplitude, area) agree with the expected values.
- A path forward to convert single-event IRFs to current integrated has been developed

Back-up slides

Intensity plots for the Photek PMT240 at -4.0kV

EJ232

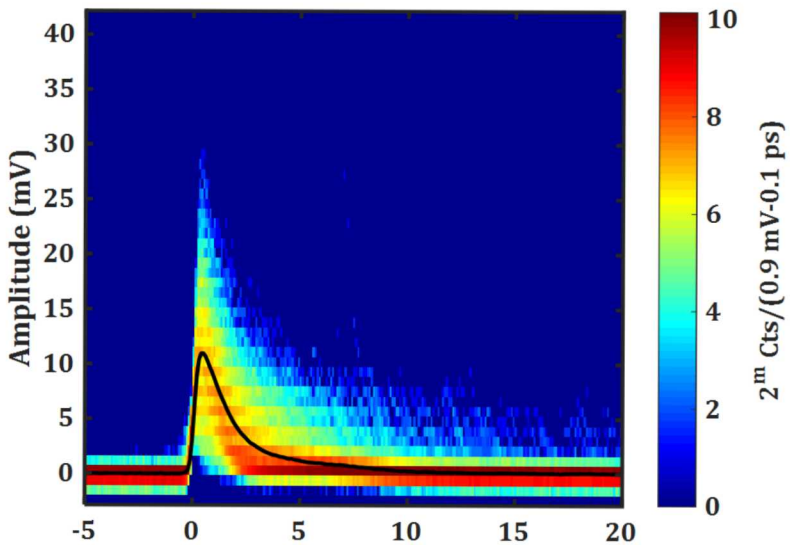

Quartz run 1

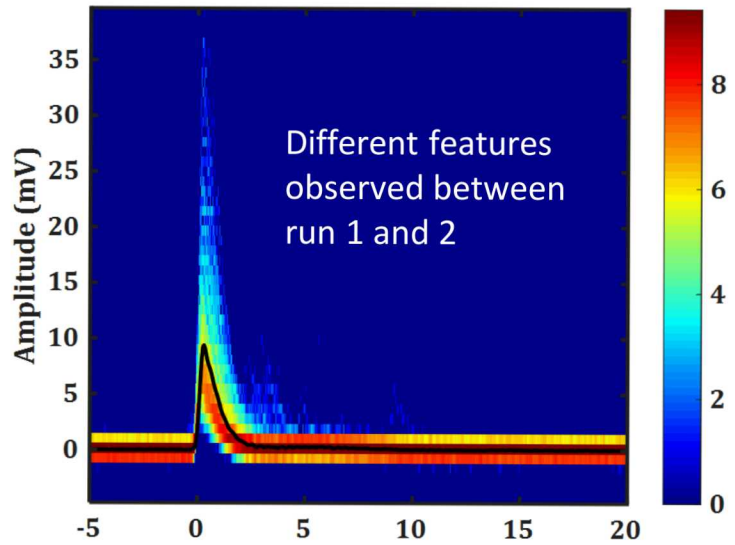

Different features observed between run 1 and 2

Quartz run2

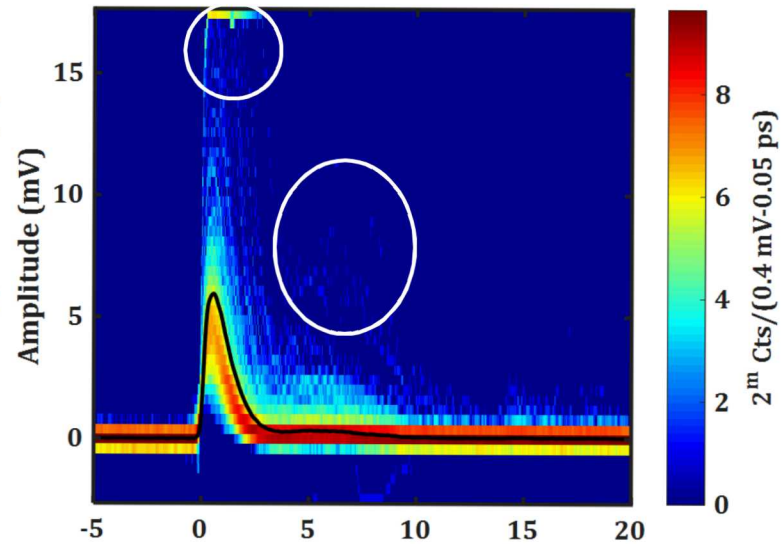

IRF measurements were made with the NTF22D-Hamamatsu mod-5 detector fitted with EJ228, EJ232Q(1%) scintillators, and quartz.

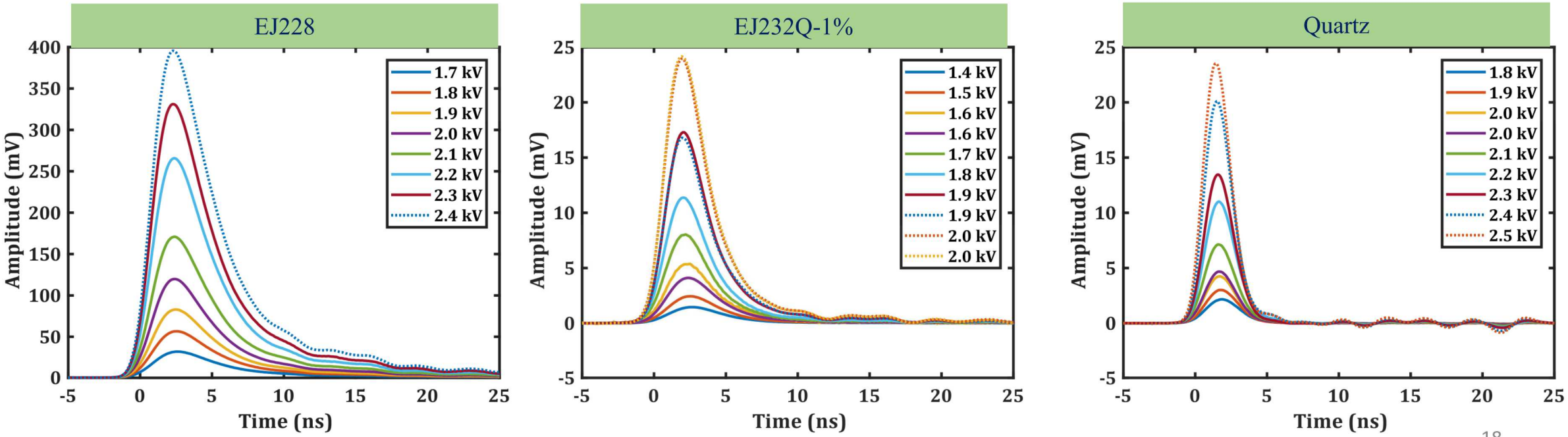

IRF measurements were made with the NTF22D-Hamamatsu mod-5 detector fitted with EJ228, EJ232Q(1%) scintillators, and quartz.

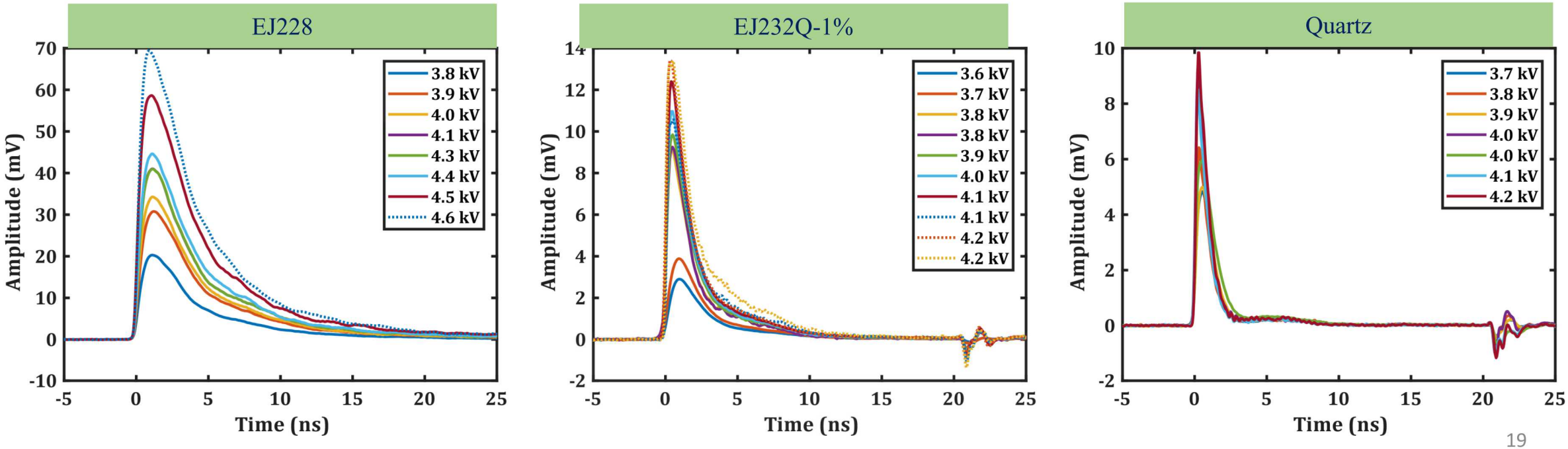

Comparison of three active detection materials for DT neutrons using NTF22D-Photek PMT240.

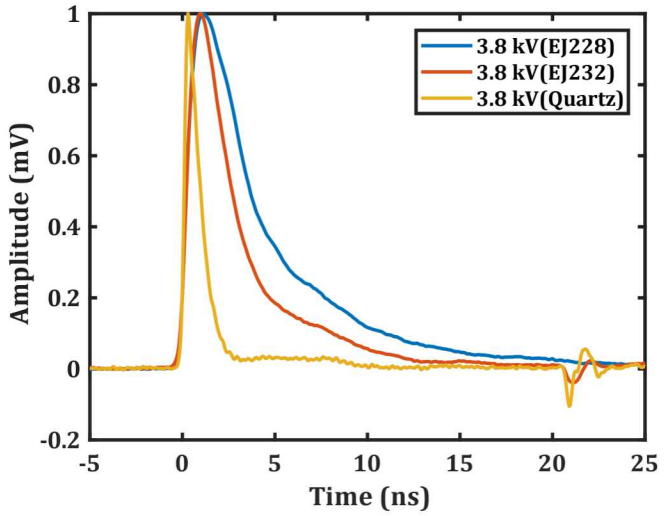

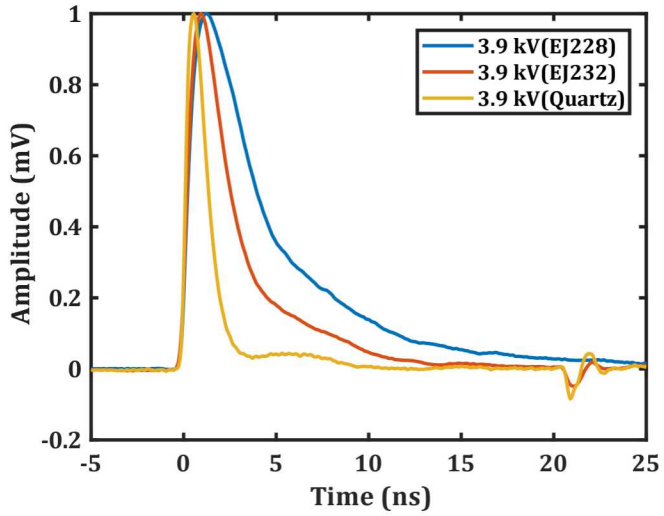

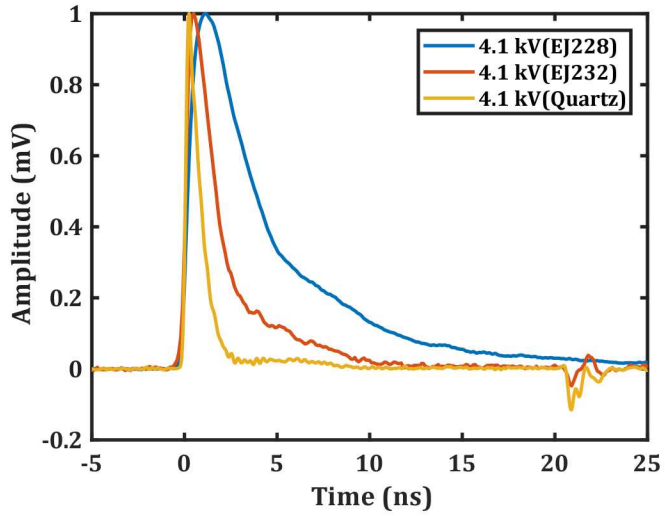

Counts were taken with NTF22D-Hamamatsu mod-5 in various configurations to determine the origin of events.

Counts for the various configurations shown on the previous slide. Counts with the quartz were repeated.

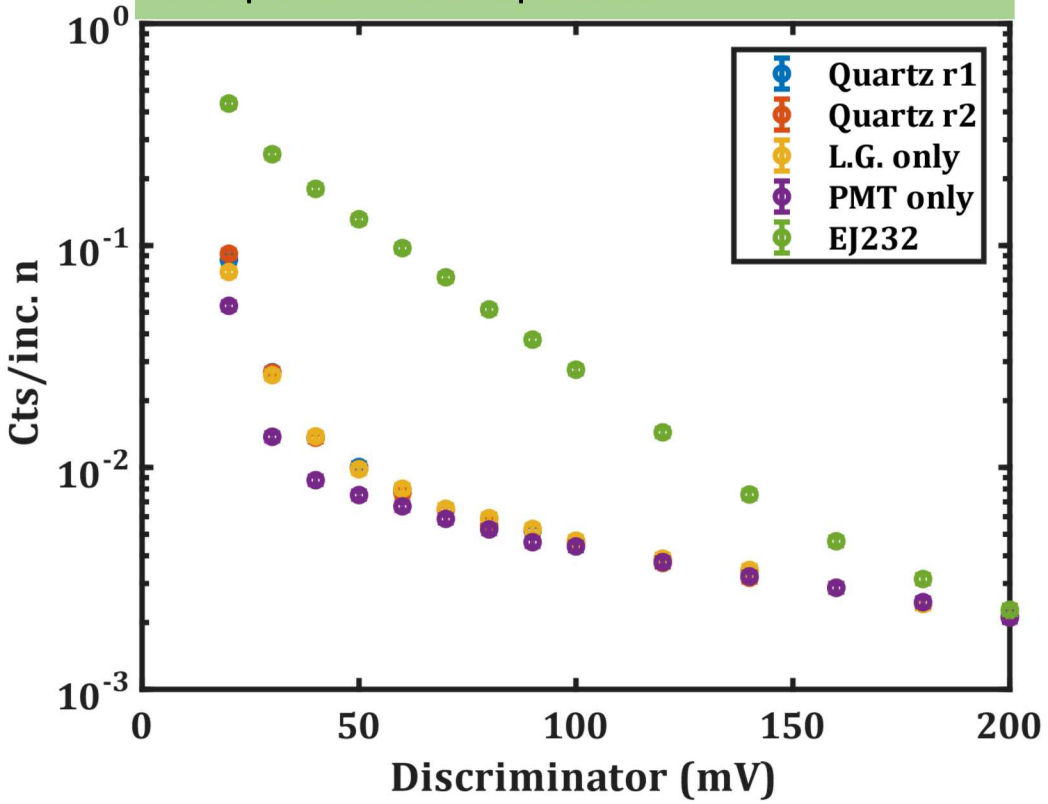

- The count rates observed with the EJ232Q-1% scintillator are an order of magnitude greater than the quartz over a substantial range of pulse heights
- The count rates observed with the light-guide and PMT only geometries are of the same magnitude as the count rates observed with the quartz in place

The number of events per incident neutron for each component can be determined by process of elimination.

$$Quartz_{r1} = Cts_{Quartz} - Cts_{light\ guide}$$

$$Quartz_{r2} = Cts_{Quartz_{r2}} - Cts_{lightguide}$$

$$Light\ guide = Cts_{light\ guide} - Cts_{PMT}$$

$$PMT = Cts_{PMT}$$

$$EJ232 = Cts_{EJ232} - Cts_{lightguide}$$

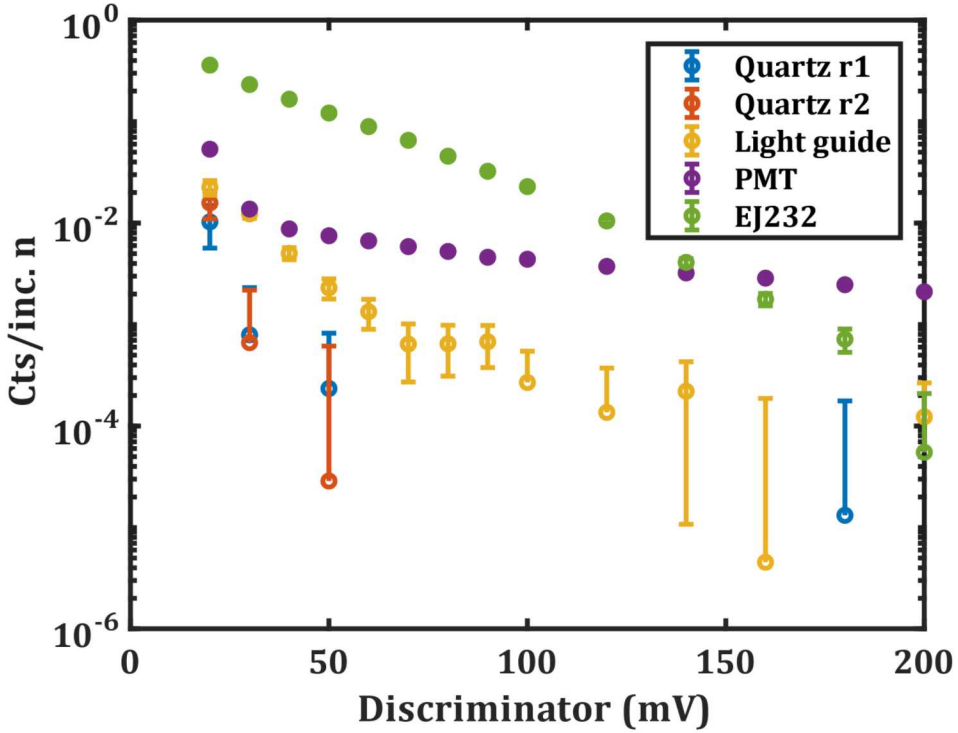

- At 50 mV the EJ232Q-1% scintillator is ~10^3 times more sensitive than the Quartz
- The PMT is ~10^2 times more sensitive than the quartz in this geometry
- At the most sensitive setting (20 mV) the EJ232Q-1% has a 20% efficiency (12% inferred from the coincidence measurement)
  - The results of this experiment, while not exact, is a good indicator of the DT neutron efficiency

A better comparison is to show the fraction of the total counts by each component as a function of discriminator.

- The PMT contribution dominates a large fraction of the signals measured with the quartz configuration
  - Shielding the PMT and light guide are absolutely essential to ensuring a neutron measurement
- The EJ232Q-1% configuration shows an expected trend. The scintillator signal dominates the lower amplitude regime (i.e. neutrons) and the PMT dominates the higher amplitude regime (i.e. photons)

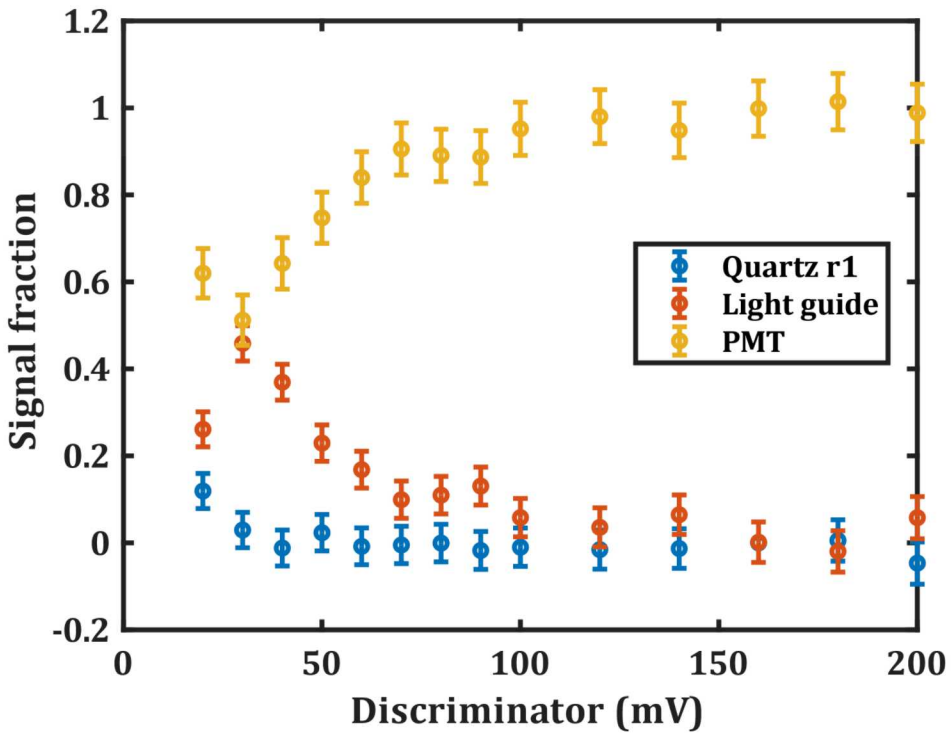

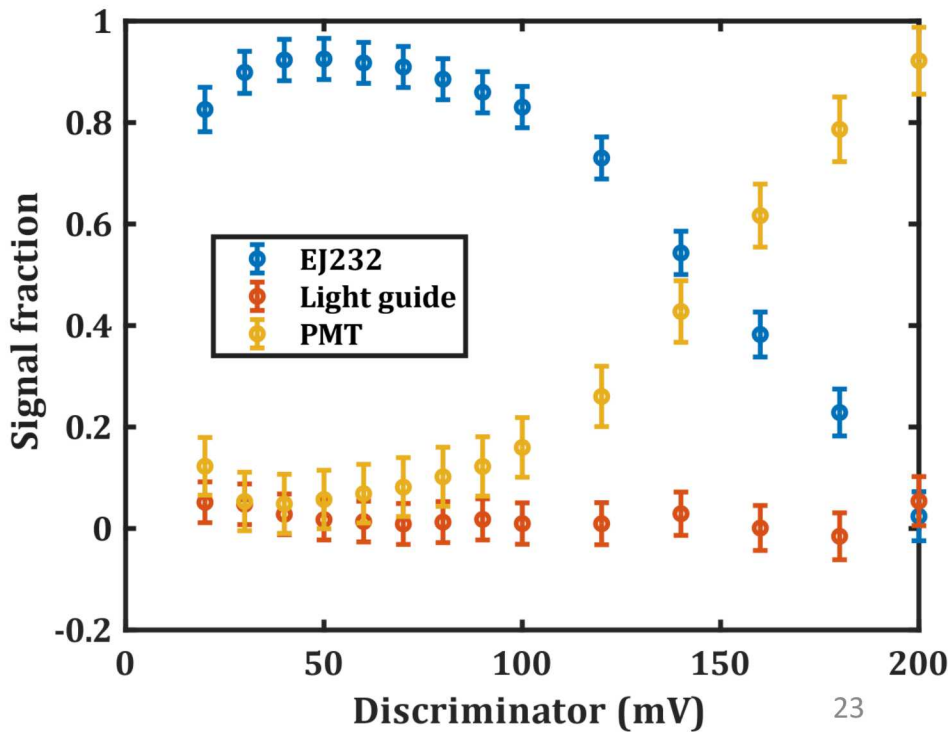

Counts and net counts for the Photek-PMT240 at -4.0 kV

Raw counts

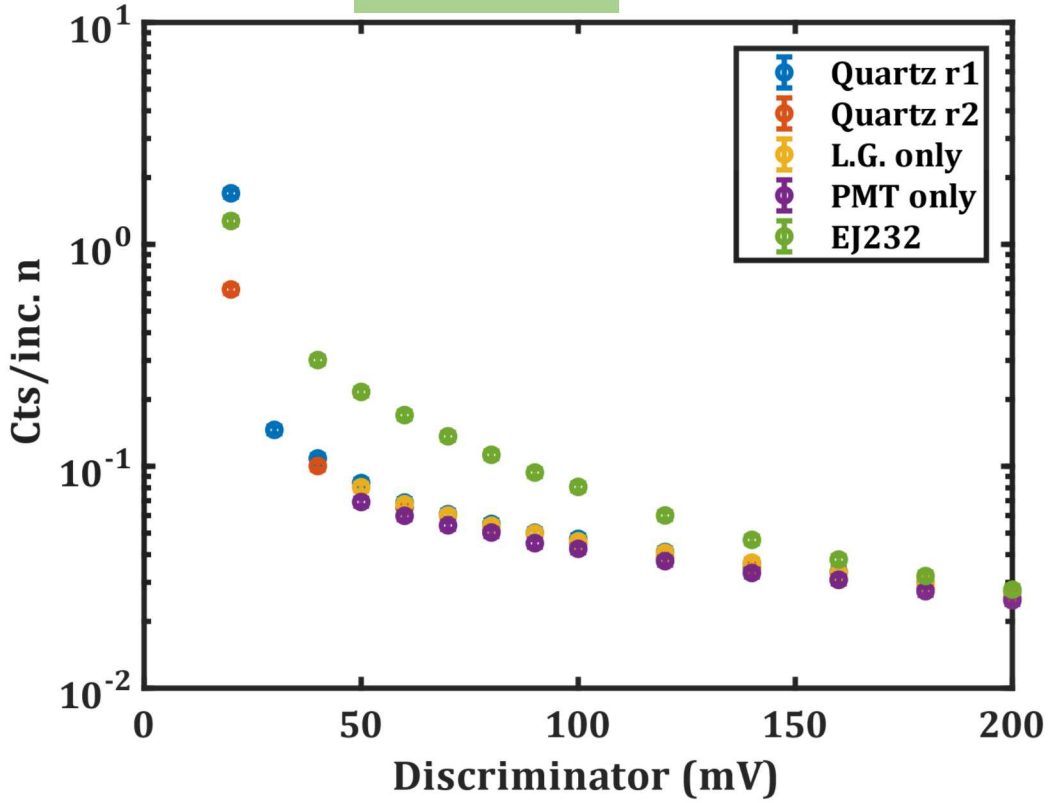

Net counts

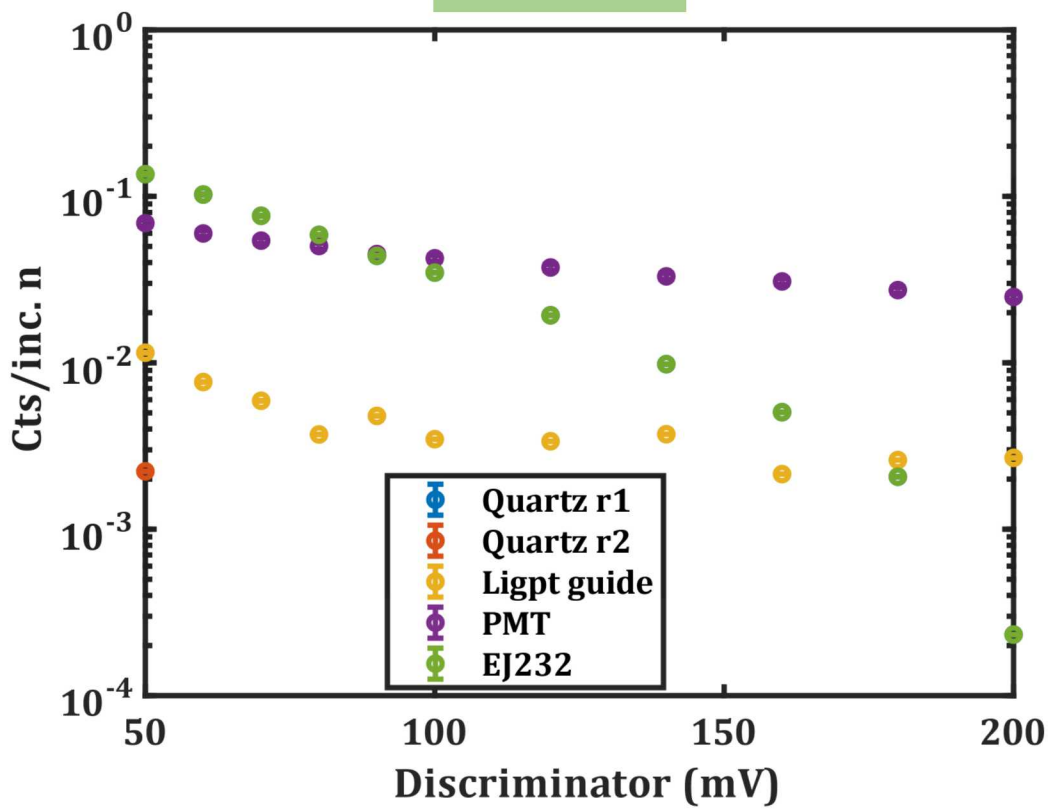

The fraction of the signal from each component as determined from the previous efficiencies for a quartz crystal and EJ232Q.

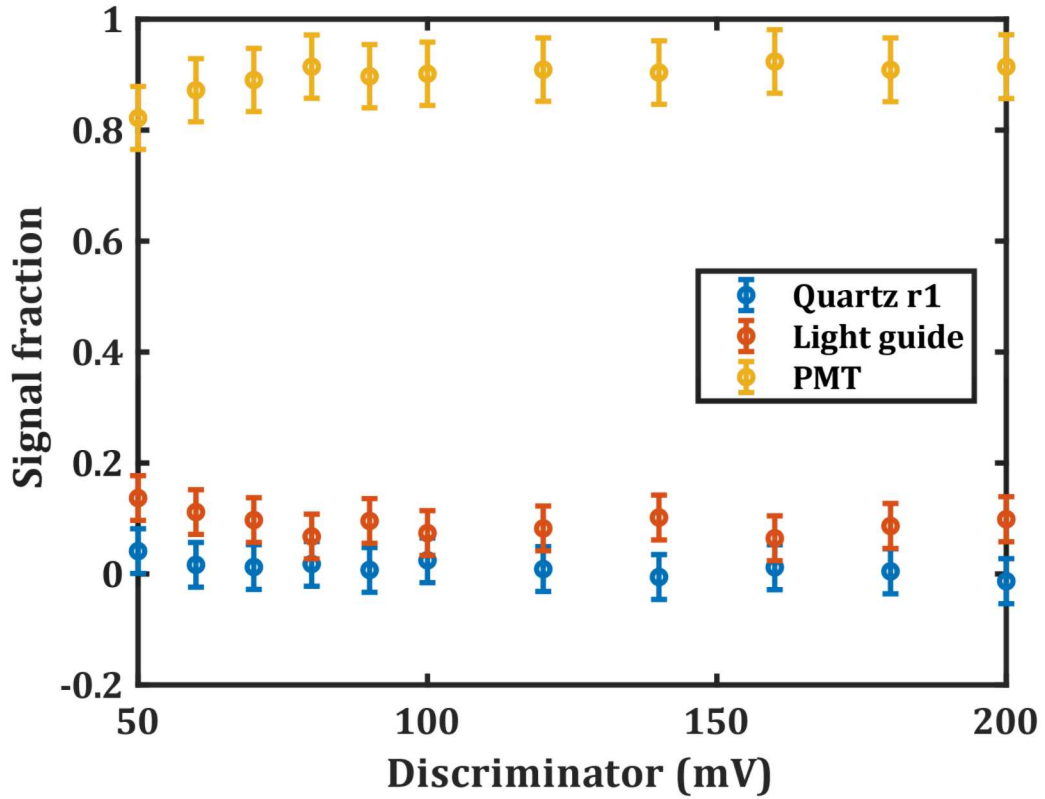

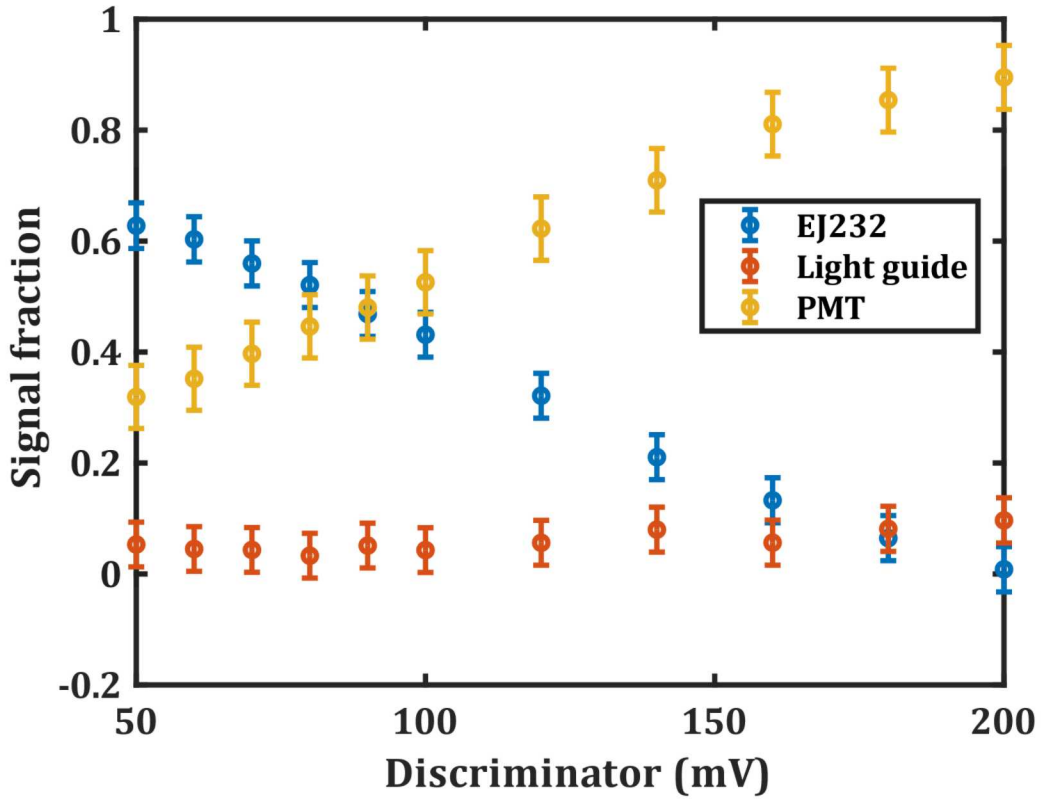

Counts were also taken directly from the PMT (split signal to o-scope and constant fraction discriminator)

Photek at -4.0 kV

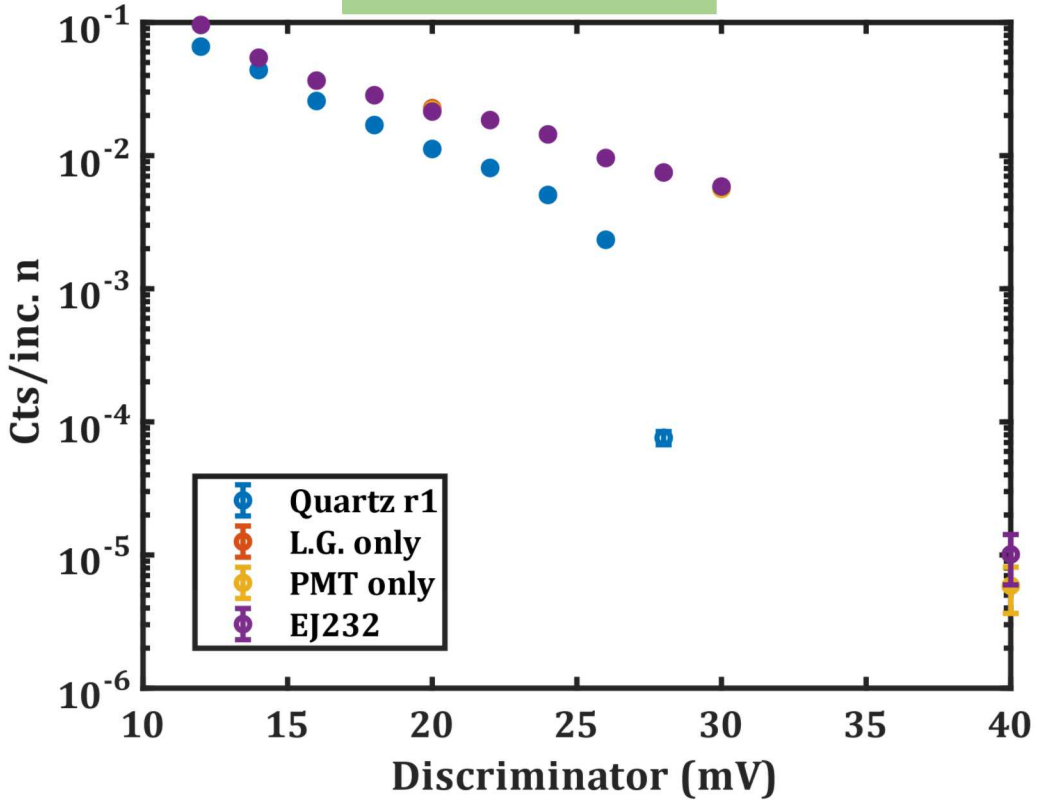

Hamamatsu at -2.0 kV

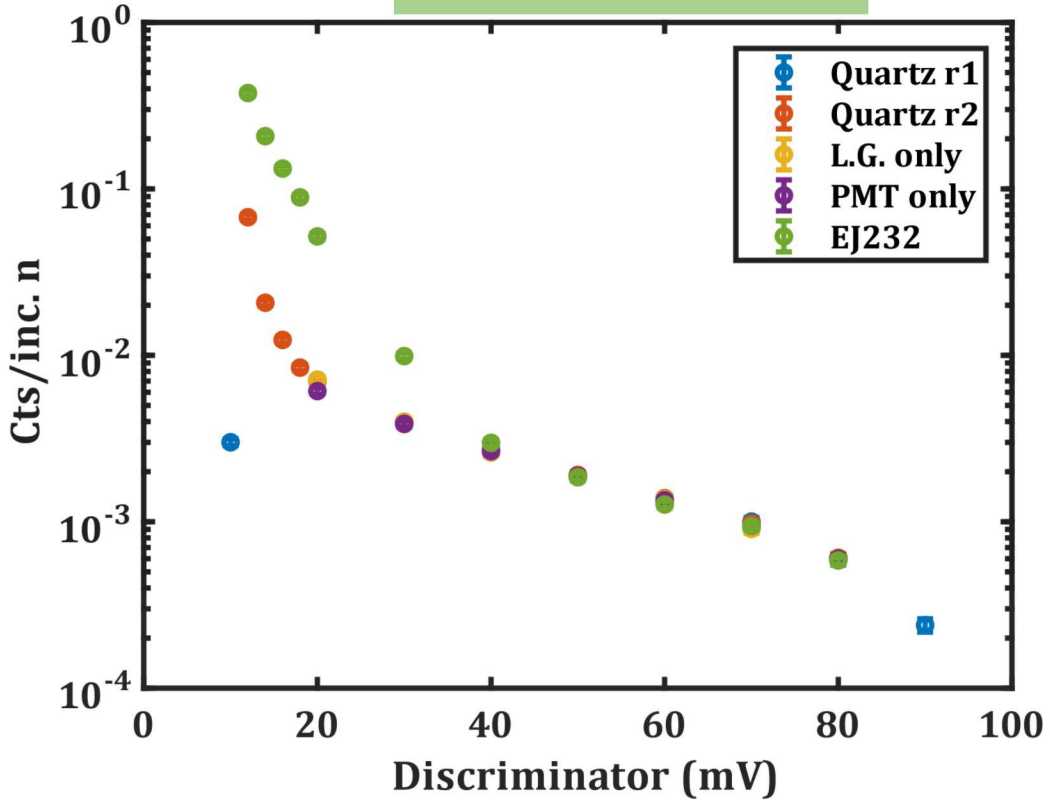

nToF characterization at the IBL includes extracting, from the same measurement, the instrument response function, the average neutron sensitivity and counting efficiency.

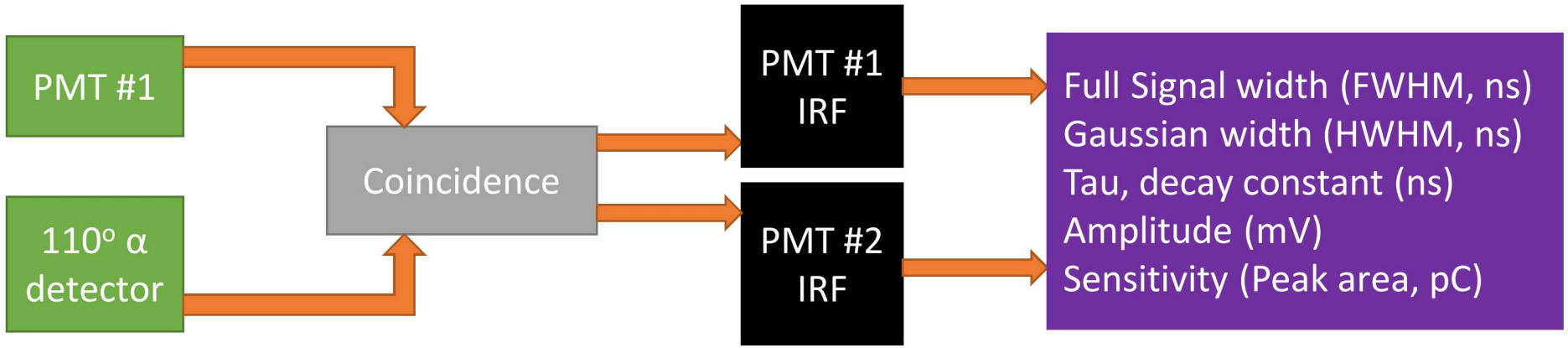

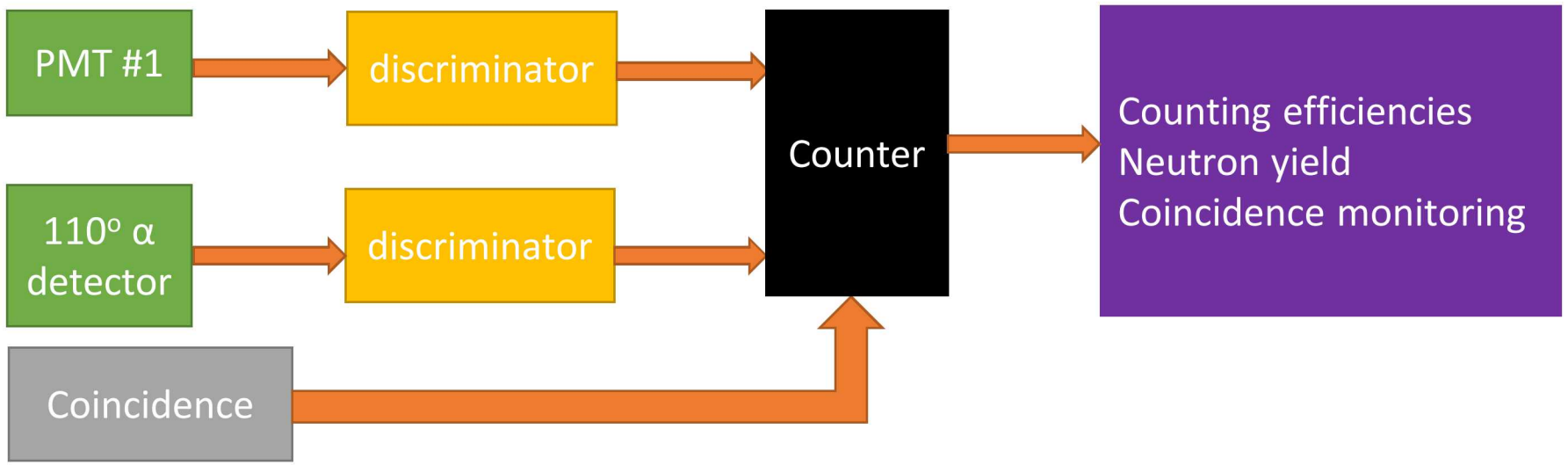

Particle coincidence is derived from relativistic two body kinematics.

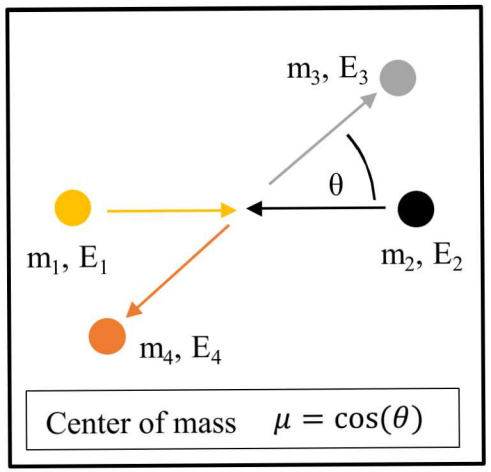

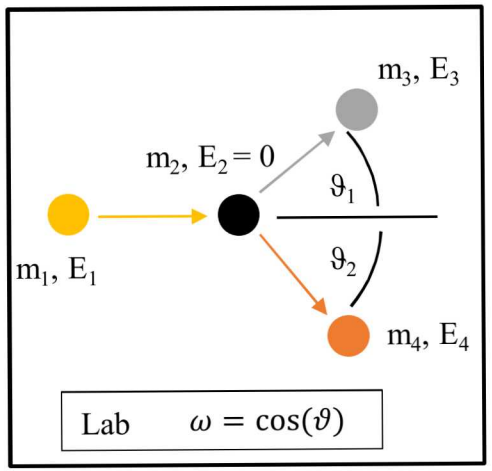

$$s_i = m_1 + m_2$$

$$s_f = m_3 + m_4$$

$$d_f = m_3 - m_4$$

$$d_i = m_1 - m_2$$

$$s = s_i^2 + 2m_2E_1$$

$$k_i^2 = \frac{(s - s_i^2)(s - d_i^2)}{4s}$$

$$k_f^2 = \frac{(s - s_f^2)(s - d_f^2)}{4s}$$

$$z_2 = \sqrt{k_i^2 + m_2^2}$$

$$z_3 = \sqrt{k_f^2 + m_3^2}$$

$$z_4 = \sqrt{k_f^2 + m_4^2}$$

$$E_3 = \frac{\left(z_2z_3 - \sqrt{k_i^2k_f^2\mu}\right)}{m_2} - m3$$

$$E_4 = \frac{\left(z_2z_4 - \sqrt{k_i^2k_f^2\mu}\right)}{m_2} - m4$$

$$P_1^2 = E_1^2 + 2m_1E_1$$

$$P_3^2 = E_3^2 + 2m_3E_3$$

$$P_4^2 = E_4^2 + 2m_4E_4$$

$$\omega_4 = \frac{(E_1 + s_i)(E_4 + m_4) - z_4\sqrt{s}}{\sqrt{P_1^2P_4^2}}$$

$$\omega_3 = \frac{(E_1 + s_i)(E_3 + m_3) - z_3\sqrt{s}}{\sqrt{P_1^2P_3^2}}$$

Uncertainty in each data point is derived from the bit-noise distribution prior to the leading edge of the waveform.

- Bit noise is defined by 11 discrete values that are normally distributed.
- 1E6 bins used for distribution; only 11 bins had counts > 0.

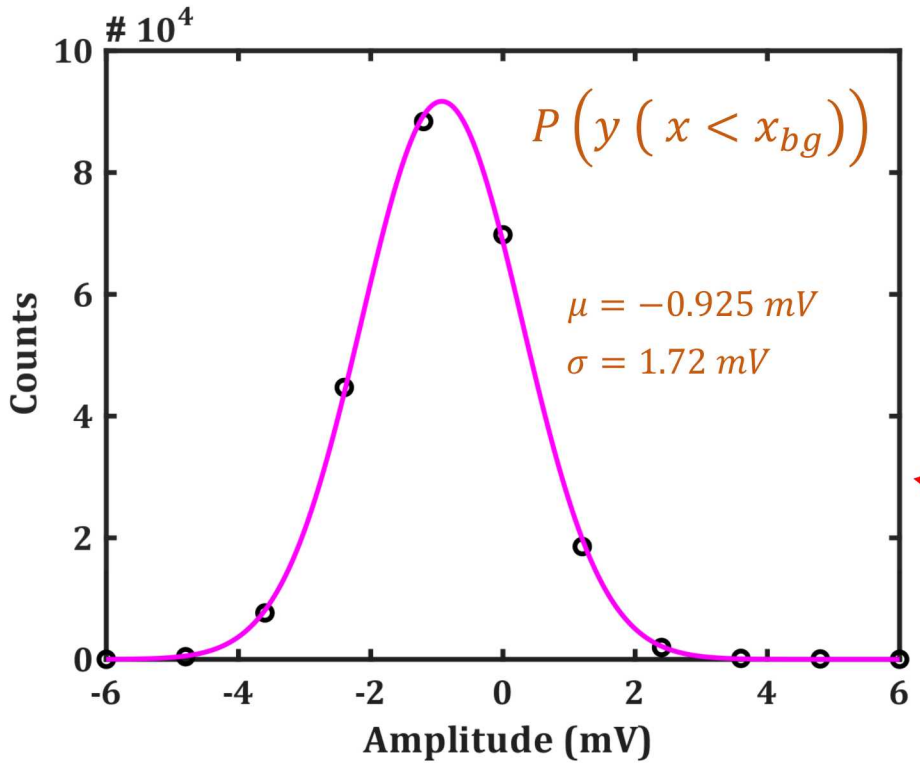

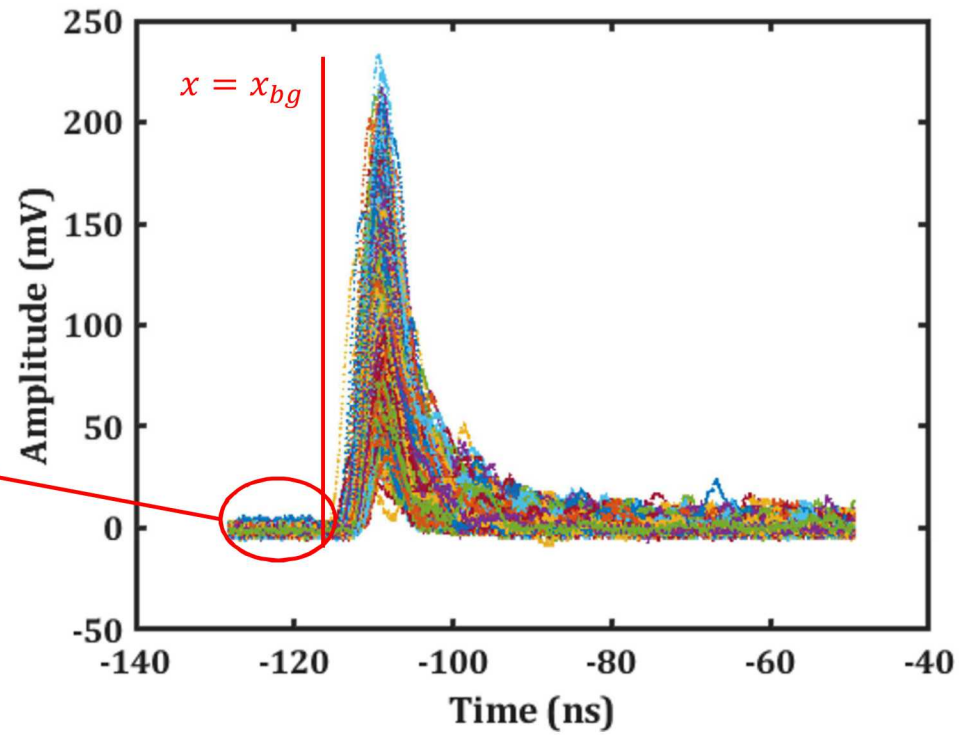

*1000 waveforms taken with NTF22D Hamamatsu mod-5 (-2.0kV), EJ228 scintillator and D-T neutrons

The uncertainty in each data point is propagated throughout the normalization process

Uncertainty in each data point

$$\sigma_y = \sigma_{noise}$$

Baseline correction

$$y_{adj} = y - y_{bl} \therefore \sigma_{yadj} = \sqrt{2}\sigma_y$$

Normalization value in y (10% of max)

$$y_n = 0.1 y_{max}$$

$$\sigma_{yn} = \sqrt{\left(\sigma_{yadj}^2 + 0.1^2 \sigma_{yadj}^2\right)} = 1.01\sigma_{yadj}$$

Normalization in x (x = 0 at 10% of maximum in y)

$$x_{norm} = x - x_n$$

$$\sigma_{xnorm} = \sqrt{\left[\left(\frac{dx}{dy}\right)^2 \sigma_{yn}^2\right]_{yn} + \left[\left(\frac{dx}{dy}\right)^2 \sigma_{yadj}^2\right]_{yi}}$$

$$\sigma_{ynorm} = \sqrt{\left(\frac{dy}{dx}\right)^2 \sigma_{xnorm}^2} = \left[\frac{dy}{dx}\sigma_{xnorm}\right]_{xi} \approx 2\sigma_y$$

Average waveform

$$y_{avg} = \sum y_{norm_i} \qquad \sigma_{yavg} = \sqrt{\frac{\sum \sigma_{ynorm_j}^2}{N}}$$

$$\sigma_{xavg} = \frac{dx}{dy}\sigma_{yavg}$$